Accepted Manuscript

Title: Organic Liquid Mobility Induced by Smoldering Remediation

Author: L. Kinsman J.L. Torero J.I. Gerhard

Please cite this article as: L.Kinsman, J.L.Torero, J.I.Gerhard, Organic Liquid Mobility Induced by Smoldering Remediation, Journal of Hazardous Materials http://dx.doi.org/10.1016/j.jhazmat.2016.11.049

Organic Liquid Mobility Induced by Smoldering Remediation

L. Kinsman[1], J. L. Torero[2], and J. I. Gerhard[1*]

[1]Department of Civil and Environmental Engineering, University of Western Ontario, London, Ontario N6A 5B9, Canada

[2]School of Civil Engineering, University of Queensland, St. Lucia Campus, Brisbane 4067, Australia

*Corresponding author email: jgerhard@uwo.ca

Highlights:

- Organic liquid waste (in sand) can be destroyed vis self-sustaining smoldering
- Under certain conditions the organic liquid migrates downwards into the reaction
- Liquid migration depends on air flow rate, system height, and liquid viscosity
- The migrating liquid influences, but does not penetrate, the smoldering reaction
- Organic liquid migration can be prevented by applying a predictable air flow rate

Abstract

Laboratory column experiments plus analytical and numerical modeling together suggest that, under certain conditions, downward organic liquid mobilization can occur and impact smoldering behavior. This applies for organic liquids mixed with inert sand subjected to smoldering as thermal treatment. The observed effects include increased peak temperatures (here by up to 35%) and increased treatment times (here by up to 30%). Downward organic liquid migration occurs when (i) injected Darcy air flux is less than a threshold value (here less than 3 cm/s), (ii) treatment systems are tall (here 90 cm, not 30 cm), and (iii) the organic liquid is temperature-sensitive (viscosity less than 0.01 Pa.s at 150° C). The developed analytical equation provides the applied air flux that can negate the downwards organic liquid gradient required for migration. Smoldering behavior is demonstrated to adjust to liquid migration and thereby still destroy all the organic waste in the system. Smoldering is a relatively new, energy-efficient thermal treatment for organic liquid waste and these results are important for designing field applications of smoldering treatment.

Keywords

1   Introduction

Lagoons containing hazardous, organic liquids are ubiquitous and present a significant environmental challenge [1, 2]. Oil sludge associated with the petroleum industry, for example, is generated at a rate of 60 million tons per year and more than 1 billion tons have accumulated worldwide [2]. Coal tar, a byproduct of coal carbonization, is another example; in 2006 China alone produced 9×10^9 kg of coal tar, representing 3.8% of the coal feed stock [3]. These are both examples of organic liquid wastes from industrial activities that are stockpiled in large quantities in lagoons and for which there are no solutions that are cost effective and technically efficient [1].

Organic liquids, when embedded in a porous medium, can be destroyed via smoldering combustion. This concept was recently introduced as a promising remediation approach for contaminated soil [4, 5]. Smoldering for the destruction of organic liquid wastes is possible but requires the liquids to be mixed intentionally with an inert porous matrix, such as sand [6]. While not participating directly in the reaction, the sand provides important physical characteristics, such as air permeability, as well as thermal properties, such as heat retention [7, 8]. This facilitates the smoldering of the liquids embedded in the pores of the matrix, destroying the liquids and leaving clean sand behind [4].

Smoldering is a flameless, exothermic oxidation reaction occurring on the surface of a condensed-phase fuel [9]. Combustion requires the combined presence of heat, organic compounds, and oxygen and converts the latter two to primarily energy, water, and CO_2. The majority of smoldering research focused on solid fuels (e.g., polyurethane foam, coal, peat) in the context of fire safety engineering [10, 11]. Intentional smoldering of organic liquid/sand mixtures as a treatment method is a relatively new concept [6]. To ignite a smoldering reaction

in these mixtures, a short and localized heat source is applied, followed by air injection [12]. Then the heat source is removed, since the organic liquid's combustion generates sufficient heat to make the reaction self-sustaining. The self-sustaining nature of the reaction underpins its potential for minimizing energy consumption and cost.

 Smoldering remediation of contaminated subsurface soils has been demonstrated at the laboratory scale [4] and scaled-up as an in situ technology applied at contaminated sites [13]. Smoldering of organic liquid waste intentionally mixed with sand has been demonstrated at the scales of a laboratory column, an oil drum, and a pilot ex situ reactor [6]. The majority of this research has focused on engineering controls and process optimization, with less known about the underpinning processes. The potential for thermal mobilization of organic liquids has been extensively studied in in the context of oil recovery [14] but it has never been studied for smoldering remediation. The time scales and structure of the oil recovery and smoldering thermal waves are different resulting in a very different balance of heat transfer modes [8]. This will affect thermal mobilization and motivate its study for the specific application of smoldering.

Smoldering is a complex phenomenon that depends on the balance between the rates and dominant modes of heat transfer and the rates and stoichiometry of suites of reactions [15, 16]. The net effect is reflected in the temperature distribution, which is the main (and often only) metric available to monitor the smoldering reaction. Fig. 1 (black curve) illustrates the distribution of temperature for a typical smoldering reaction travelling upwards in a one-dimensional column. In this context, the column contains a high-viscosity organic liquid (e.g., coal tar, oil sludge) mixed intentionally with quartz sand to a specified saturation (e.g., 50%) with the remaining porosity occupied by air. Peak smoldering temperatures for these liquids are typically 700-1000°C [6].

Of key interest in this work is the preheating region, which has temperatures in the range of 50 – 200°C, where the sand/organic mixture is absorbing energy transmitted from the smoldering reaction below. Here exists the potential for organic liquid mobilization. Organic liquid is expected to migrate at a certain velocity (v_O) that, following Darcy's Law, depends on its viscosity and hydraulic gradient. At ambient temperatures, the high viscosity of long chain hydrocarbons means migration is slow even in the presence of significant hydraulic gradients [17]. However, liquid viscosity decreases rapidly with increasing temperatures [18]. Fig. 2 presents the sensitivity of liquid viscosity to temperature for a range of organic liquids used in this work and related studies. It reveals that viscosity may decrease by a factor of 10 to 1,000,000 over this temperature range, i.e., 50 – 200°C, and the sensitivity is dependent on organic composition. Therefore, v_O may be significant in the preheating region.

Reduction of organic liquid viscosity leading to mobilization is intentional for applications such as in situ combustion for enhanced oil recovery [14] and steam injection for remediation [19]. In the context of smoldering destruction of organic liquids, any mobilization is unintentional. It is potentially undesirable and its effects are unknown. Moreover, it is impossible to monitor directly: there is no known technique for tracking organic liquid saturation in such hot systems. Any liquid mobilization is expected to be expressed in the temperature profile. A secondary impact could be the presence of residual organic remaining behind the front if mobilized liquid is able to penetrate the reaction into the normally clean sand below.

The objective of this work was to explore the relationship between organic liquid smoldering and mobilization. It explores the conditions that lead to liquid mobility and the subsequent influence on the key metrics of smoldering remediation. Laboratory column experiments of organic liquid smoldering were conducted using columns of varying height. Because temperature was the only

direct observation available during smoldering, additional information on organic liquid migration was obtained using modeling. An analytical model was developed to explain the relationship between organic liquid mobility and injected air flow rate. Numerical modeling was employed to explain the role of liquid viscosity. The improved understanding provided in this work of organic liquid mobility in the context of smoldering remediation will aid in the design and implementation of commercial applications of this technology currently underway.

2 Materials and Methods

2.1 Experimental Setup

Smoldering experiments were conducted in an upwards, 'forward' smoldering mode (i.e., air flow travelling in the same direction as the reaction). The two stainless steel columns were 16 cm in diameter, with the shorter column containing a 30 cm organic liquid-contaminated zone, and the taller column containing a 90 cm organic liquid-contaminated zone. The experimental setup was based upon the standard configuration [4, 7,]. A schematic of the 30 cm column is shown in Fig. 3. The 90 cm column was identical except for the height of the contaminated zone and the presence of 26 thermocouples instead of 9.

An air diffuser was placed in the bottom of the column and connected to the compressed house air supply. An inconel-sheathed electrical cable heater (Watlow, USA, 450 W) was coiled into a flat spiral and placed above the air diffuser. Clean sand filled the base until covering the heater by a few millimetres. The quartz sand (#12ST, Bell and Mackenzie Co. Ltd., Canada) used in all experiments had a bulk dry density of 1600 kg/m^3 and mean grain size of 0.88 mm. A 30 cm (or 90 cm) layer of the contaminated material was packed and tamped in 10 cm lifts above the diffuser and heater.

The organic liquid used was a homogeneous (single phase) mixture (50:50 by mass) of canola oil and viscosity index improver (V-158, Tempo Canada ULC). Canola oil was used because it will sustain smoldering and is non-toxic. However, its ambient temperature viscosity is relatively low (0.1 Pa·s, Fig. 2). With the addition of viscosity index improver, the organic liquid waste surrogate exhibited a viscosity (1 Pa·s) much more representative of lagoon wastes such as coal tar and crude oil (Fig. 2). While the temperature dependence of the surrogate's viscosity is not known, due to equipment limitations, it is expected that it declines to approximately 0.01 Pa·s above 100°C like all other organic liquids for which we have data (Fig. 2). The contaminated material packed in the columns was prepared by mechanically mixing (KitchenAid, Pro Line) the desired mass ratio of organic liquid to sand, 60 g/kg, until homogeneous. This mimics the method used in industrial applications of smoldering to treat lagoon wastes. The mass added provides a target, nominal organic liquid saturation of 0.30, based on an average measured sand porosity of 0.38. A preliminary experiment confirmed that this organic liquid did not migrate under ambient conditions (Appendix A). The rest of the pore space contained air; no water was included. The minor impact of water on these smoldering systems has been documented in numerous studies [13] and is therefore not expected to be a significant factor here.

Inconel-sheathed type K thermocouples spaced at 3.5 cm intervals were placed along the centreline of the contaminated zone, with the first thermocouple (TC1) located 1.0 cm above the heater. The thermocouples were connected to a data acquisition system (Multifunction Switch/Measure Unit 34980A, Agilent Technologies) and a personal computer to record data at two-second intervals. This is the standard approach for tracking smoldering reactions (e.g., [26]). Insulation (2" mineral wool, McMaster-Carr) encircled the columns to minimize heat losses. Although the column was insulated, some heat losses still occur at the boundary likely

leading to temperatures approximately 100° C lower at the wall of the column than along the centerline. While this temperature gradient may lead to slight curvature of the smoldering front, these effects are considered to be minimal in a column system and are expected to only decrease further with increasing scale.

A standard ignition procedure was employed [4]. The heater power was increased in 25 W increments every 10 minutes from an initial power of 290 W to 415 W, at which point the heater power was maintained until the first thermocouple (TC1) reached 360˚C (approximately 90 min from the start of heating). The air supply was then initiated and maintained until completion of the experiment. The heater was turned off after TC1 reached its peak temperature, approximately five minutes after the start of air flow; thus, from this time onwards, the smoldering reaction propagated in a self-sustaining manner. The air flow through the column was regulated using a mass flow controller (FMA5544, Omega). The inlet (Darcy) air flux reported for all experiments was calculated by dividing the volumetric flow rate at standard temperature and pressure by the horizontal cross-sectional area of the column.
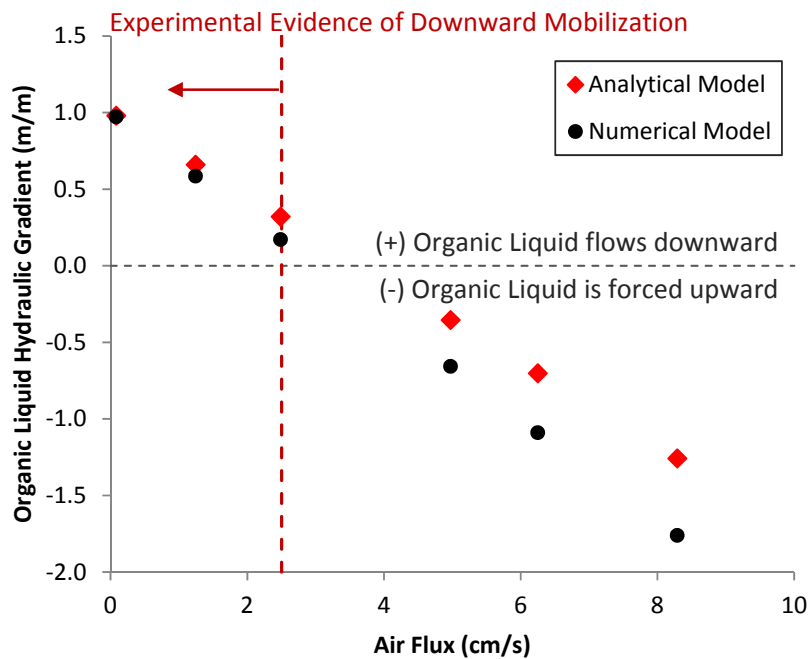
Fig. 11. Organic liquid hydraulic gradient as a function of forced air flux represented as black circles for the numerical simulations of a 90 cm contaminated zone with a 10 cm preheating zone immediately above the front (A = 80, B = 10, C = 0). Organic liquid hydraulic gradients calculated using the analytical model are shown in red.
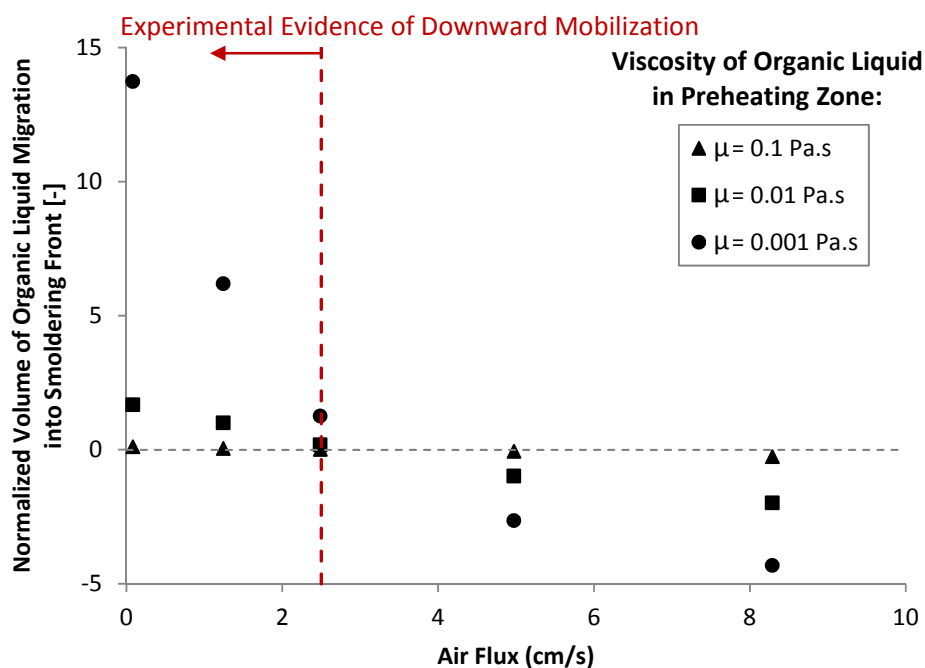
Fig. 12. Volume of organic liquid entering (+) or leaving (-) the bottom 10 cm of a 90 cm column over 20 minutes as a function of (i) forced air flux and (ii) viscosity of the organic liquid in the preheating zone. Simulation results are for a 10 cm high preheating zone located at the base of an 80 cm ambient, organic liquid-contaminated zone ($\mu = 0.5$ Pa·s), where A = 80, B = 10 and C = 0. Volumes are normalized relative to the base case (1.25 cm/s flux, $\mu = 0.01$ Pa·s).

Table 1 outlines the six experiments conducted.

In order to compare smoldering behavior in different sized columns, temperatures were plotted against dimensionless time:

$$DT = t(\frac{v_s}{L})$$

where DT is dimensionless time, t is time, v_s is the average smoldering velocity, and L is the length of the contaminated zone. The average smoldering velocity is defined as the average of all the local smoldering propagation velocities throughout the experiment. Each local velocity was determined from the time lapse of the front arrival (i.e., temperature spike) at two consecutive thermocouples and the known distance between them [26].

2.2 Analytical Model

Assuming negligible capillary pressure under forced airflow conditions, atmospheric pressure at the top of the column, and approximating the air pressure at the base of the column with the Kozeny-Carman equation [27], which combines Poiseuille's equation for laminar flow with a capillary tube bundle model and assuming spherical uniform particles, provides (complete derivation shown in Appendix B):

$$\frac{\Delta h}{\Delta L} \approx 1 - \frac{\left[\frac{180V\mu_A}{\varphi_s^2 D_p^2}\right]\left[\frac{(1-\varepsilon)^2}{\varepsilon^3}\right]}{\rho_{OL} \cdot g} \qquad \text{(Eq. 2)}$$

where h is the total hydraulic head of the organic liquid, $\Delta L = L$ is the length of the contaminated zone given that the datum is considered to be the base of the column, V is the Darcy air flux (volumetric flow rate divided by cross-sectional area of the column), μ_A is the dynamic viscosity

of air, φ_s is the sphericity of the particles in the column, D_p is the mean diameter of the particles,

ε is the effective air porosity (total porosity minus the percent volume occupied by organic

liquid), ρ is density, and g is gravitational acceleration. Recall that liquid flow occurs in

response to a hydraulic gradient [28]. If the hydraulic gradient calculated using Eq. 2 is positive

then the potential exists for downward organic liquid mobilization (see Appendix B for more

information). Eq. 2 indicates that the organic liquid hydraulic gradient depends primarily on the

injected air flux and is independent of the height of the column.

For the organic liquid and sand used in this study, the parameters for Eq. 2 are provided in Table

2.

2.3 Numerical Model

To investigate the time-dependent potential for organic liquid migration, a numerical model was

employed. A one-dimensional version of the finite difference, two-phase flow model DNAPL3D

[33-37] was employed. The model solves the organic liquid and air mass conservation

equations, which include Darcy's Law, fluid incompressibility assumptions, the capillary

pressure definition $P_C = P_A - P_{OL}$, and the fluid saturation relationship $S_{OL} + S_A = 1.0$:

$$\frac{\partial}{\partial z}\left[\frac{k_i k_{r,OL}}{\mu_{OL}}\left(\frac{\partial P_{OL}}{\partial z} + \rho_{OL}g\right)\right] - \emptyset\frac{\partial S_{OL}}{\partial t} = 0 \qquad \text{(Eq. 3)}$$

$$\frac{\partial}{\partial z}\left[\frac{k_i k_{r,A}}{\mu_A}\left(\frac{\partial (P_C + P_{OL})}{\partial z} + \rho_A g\right)\right] - \emptyset\frac{\partial (1 - S_{OL})}{\partial t} = 0 \qquad \text{(Eq. 4)}$$

where z is the vertical coordinate, k_i is the intrinsic permeability, $k_{r,OL}$ and $k_{r,A}$ represent the

relative permeability of the organic liquid and air, respectively, μ_{OL} and μ_A represent the viscosity

of the organic liquid and air, respectively, P_{OL} is the organic liquid pressure, P_C is the capillary

pressure, ρ_{OL} and ρ_A represent the organic liquid and air phase densities, respectively, g is gravitational acceleration, $\emptyset$ is the porosity, S_{OL} is the organic liquid saturation, and t is time. In this system, organic liquid is the wetting phase and air is the non-wetting phase. Capillary pressure-saturation-relative permeability functions close the system of equations [33, 34]. The pressure and saturation distributions are solved as a function of height and time within the column, subject to inertial, gravity, and capillary forces and subject to the influences of soil permeability, multi-phase relative permeability, and fluid viscosities. The model has been applied to a wide range of problems in which two immiscible fluids are flowing through a porous medium [29, 38].

The purpose of the numerical model was to simulate the migration of an organic liquid in a porous medium under conditions resulting from smoldering for a single location of the front in the column and over a limited period of time. The key factors to consider in this problem are phase hydraulic gradients (liquid and air), liquid viscosity, porous medium permeability, relative permeability, and time. Simulating smoldering itself, with all its associated complexities such as heat transfer, chemical reactions, and kinetics, are not needed to answer this specific question. Such a sophisticated model would be needed only if it was desired to simulate the dynamic interaction of smoldering and organic liquid migration as conditions changed over time (e.g., an entire experiment from start to finish). To answer the question of whether organic liquid migration is expected to occur under specific conditions at one "short interval of time" within an experiment, only a multiphase flow model such as that described is necessary.

The potential for organic liquid migration was evaluated for a single 'configuration' in each simulation. Configuration in this context means a single "short time" over which the front is effectively motionless and thus the relative lengths in the column of the preheated region and

ambient temperature region can be defined. The viscosity of the organic liquid was assigned a reduced value in the preheated region, based upon that expected to occur at approximately 100°C (Fig. 2). For each configuration (i.e., simulation) the model can only answer the question of whether organic liquid migration into the front is expected to occur and, if so, to what extent (relative to other configurations). By exploring a range of configurations (e.g., preheating zone lengths, viscosities of the heated organic liquid, front positions in the column, and air flow rates) it is possible to examine the range of conditions under which organic liquid migration is possible.

The model domain and boundary conditions, shown for one example scenario, are summarized in Fig. 4. The domain height was set to match the height of the organic liquid-contaminated zone. The domain was discretized into 2 cm nodes. The top boundary was assigned a fixed air pressure of zero, corresponding to an open-top column. The bottom boundary condition consisted of an organic liquid flux of zero, so that any downward migrating organic liquid would accumulate and could be quantified. It also specified an air flux matching the injected air flow rate for each simulated experimental condition.

Table 3 provides the model input parameters. The parameters with the expected highest sensitivity were measured in the laboratory including: organic liquid viscosity and saturation, and soil porosity and permeability; the remainder were based on literature values as outlined and referenced in Table 3. The zone of primary interest for all model simulations is the preheating region (height B in Fig. 4). Based on experimental measurements, air temperatures in this region are expected to be ~ 200°C and thus air fluid properties at that temperature were used. The effect of temperature on interfacial tension was neglected because, as expected, capillary forces are demonstrated to be negligible in this system (see Results).

Each scenario (i.e., each simulation) was run for 20 min. The typical velocity of the trailing edge of the front is 0.2-0.3 cm/min, meaning an approximately 5 cm movement of the front is expected in 20 minutes. Thus, assuming a single location of the front and single thickness of the preheating region is reasonable for these simulations.

The base case simulation used the experimental conditions of Test 4 after a dimensionless time of 0.1, when the front was located at the base of the column (see Fig. 9a). The simulated configuration therefore consisted of a 90 cm contaminated zone with a forced air flux of 1.25 cm/s, and a 10 cm preheating zone above the front. An additional 27 simulations were run, investigating the influence of four parameters: injected air flux (0.1 to 8.3 cm/s), height of the contaminated zone (16 to 120 cm), height of the preheating zone (0 and 10 cm), and the viscosity of the organic liquid within the preheating zone (0.001 to 0.1 Pa·s). Three of these simulations correspond to specific configurations representing Tests 1, 5, and 6 and allow a direct comparison between them. All of the simulation results for the volume of NAPL migration are normalized by the results of the base case.

3   Results and Discussion

3.1   Experimental Studies of Smoldering Behavior

Temperature history as a function of dimensionless time (DT) for the base case experiment, Test 2, is shown in Fig. 5. DT=0 occurs when the air supply, and therefore smoldering, was initiated. The initiation of 2.5 cm/s air flux at this time caused a distinct slope change in the rate of temperature increase, representing the onset of smoldering combustion. Once TC1 reached its peak temperature and began to decline, the heater was turned off and only the air supply remained on. The consistent and repetitive temperature-time slopes, the crossing of successive curves, and the consistency of the peak temperatures (564 ± 12 °C), are all indicative of a self-

sustaining smoldering process [12]. The velocity of the leading edge of the smoldering front is steady in time (0.41 ± 0.04 cm/min).

Fig. 6 presents the base case results as a time sequence of temperature profiles. The preheating region is defined as the region ahead of the leading edge of the smoldering front where T>100°C. While the preheating region was previously defined as a range of temperatures (50 - 200°C), a single temperature value is required to consistently define the boundary between the preheating and ambient temperature zones and allow for comparison between different cases. Due to the significance of the reduced organic liquid viscosity within the preheating zone in this study, a temperature of 100°C was selected for this purpose based on the relationship between temperature and organic liquid viscosity (Fig. 2). Smoldering front thickness was determined based on the temperature profile; an example is shown for DT=0.8 in Fig. 6. The velocity of the leading (0.41 ± 0.04 cm/min) and trailing edge (0.30 ± 0.06 cm/min) of the smoldering front were not equal in the base case experiment, resulting in an increase in the thickness of the smoldering front over time, from 1 to 10.5 cm over the approximately 80 minutes of smoldering.

The 30 cm experiments at the other two air fluxes (1.25 and 6.25 cm/s), reveal the same features as the base case, including steady progression of the leading edge of the front (0.34 ± 0.06 cm/min and 0.50 ± 0.03 cm/min, respectively), lower velocities of the trailing edge of the front (0.24 ± 0.06 cm/min and 0.35 ± 0.05 cm/min, respectively) and consistent peak temperatures (560 ± 15 °C and 573 ± 14°C, respectively). A faster and hotter reaction is expected when air flow is increased; indeed a linear dependence of smoldering front velocity on injected air flux has been shown [9] and is expected since smoldering is an oxygen-limited reaction. All of the 30 cm column results are consistent with published experiments of organic liquid smoldering at the

same scale [4, 6, 7, 13 and with solid fuel smoldering at small and large scales [9, 11]. For these reasons, this will be referred to as 'typical' smoldering behavior and is understood to be representative of no organic liquid migration.

Differences in behavior were observed when the height of the contaminated zone was increased. Fig. 7a shows the temperature history for the 90 cm column with a forced air flux of 2.5 cm/s. Typical smoldering behavior was observed from approximately TC1 to TC12, including a constant velocity of the leading edge (0.41 ± 0.07 cm/min) and trailing edge of the smoldering front (0.32 ± 0.07 cm/min), and consistent peak temperatures (564 ± 17 °C); all consistent with the 30 cm column. However, atypical behavior is observed beginning at DT=0.6. The steady progression of the front is interrupted and both dips and spikes in temperature are observed beyond this time. For example, TC14 exhibits a cooling event interrupting smoldering followed by a second ignition event. This pattern is repeated for all TCs after DT=0.6, and the temperatures of these second peaks continue to increase, as shown in Fig. 7a. The upper half of the column sees peak temperatures as high as 750 °C, far beyond the typical peak smoldering temperature. The most likely explanation for this atypical smoldering behavior is downward organic liquid migration.

The temperature profiles for this experiment, Fig. 8, reveal that in the period 0.6<DT<0.7, the trailing edge of the smoldering front stalls (i.e., velocity of 0 cm/min) while the leading edge of the front continues to advance. This corresponds to a regime change in smoldering behavior characterized by a highly accelerated growth of smoldering front thickness and elevated peak

temperatures. In order to confirm that this regime change was not an isolated incident, a repeat column test was conducted (Appendix C, Fig. C.1), yielding similar results.

These observed changes in smoldering behavior are consistent with a hypothesis of downward organic liquid migration from the preheating zone into the reaction zone. Such migration of relatively cool liquid (~200° C) into a smoldering zone (~500° C) would cause rapid, temporary temperature dips and the additional time required for this additional fuel to ignite and be consumed would cause a stall of the trailing edge of the front. It is noted that the ignition temperature of the fuel is known to be not more than 360° C, so oxidation at 500° C is not unexpected. Moreover, the concentration of energy at the front could cause higher than average peak temperatures. Such 'superadiabatic conditions' have been documented in smoldering of solid porous fuels (e.g., coal, foam) when in situ conditions, like air flow rate, allow heat to accumulate in the reaction zone [15]. This appears to be the first documented case of such conditions arising from organic liquid (i.e., fuel) migration. Fig. 1 (red curve) presents a conceptual model of how the standard temperature profile changes in such cases.

Tests 4 and 6 demonstrate that this 'atypical' smoldering behavior is sensitive to the injected air flux in the tall columns. At the lowest air flux (Fig. 9a), the atypical behavior starts immediately at the initiation of smoldering: (i) the bottom third of the column exhibits unusually high average peak temperatures higher (630 ± 22 °C), (ii) the trailing edge of the front stalls at early time, and (iii) the leading edge of the front proceeds uniformly (0.38 ± 0.07 cm/min) and the top third of the column exhibits average peak temperatures (538 ± 38 °C) that are reduced relative to typical. These are all consistent with organic liquid migration from the upper half to lower half of the column. Meanwhile, the highest airflow case in the 90 cm column exhibited none of these

characteristics (Fig. 9b), showing typical behavior including steady progression of the leading

(0.53 ± 0.04 cm/min) and trailing edges (0.45 ± 0.08 cm/min) and consistent peak temperatures

(563 ± 5 °C). Based on these results, it is hypothesized that reduced airflow rate results in an

earlier onset of downward organic liquid migration and increased airflow prevents it entirely.

Careful post-treatment excavation revealed completely clean and dry sand for all of the

experiments, consistent with greater than 99.9% organic destruction confirmed by gravimetric

TPH analyses [4]. Thus, regardless of atypical smoldering behavior, all of the liquid was

consumed via smoldering and the entire column was remediated. This is consistent with the

hypothesis, since it is expected that any organic liquid migrating from the preheated region into

the reaction will be ignited by the much higher temperatures in that region.

Fig. 10, summarizing all of the experimental results, reveals that the preheating zone thickness

never exceeded 10.5 cm in the 30 cm experiments,. In addition, both the leading and trailing

edges of the front propagated in a steady manner upwards, ensuring the thickness of the

combustion zone was relatively consistent across all airflow rates and never more than 10 cm.

For the 90 cm columns, atypical smoldering behavior was observed when the preheating zone

exceeded 10.5 cm. At the lowest injected air flux, this occurred at the onset of smoldering (DT =

0.1). The height of the preheating zone continued to expand as the reaction progressed and at

DT=0.4 the trailing edge of the smoldering front stalled. For the intermediate air flux, the

preheating zone exceeded the critical height, and the trailing edge of the front stalled,

approximately half way through the smoldering process (at DT=0.6). These times coincided

with when atypical smoldering behavior was observed (Fig. 8 and Fig. 9a, respectively). It is

hypothesized that a 10.5 cm thick preheating zone represents a critical amount of low-viscosity organic liquid, which upon migrating into the reaction zone, manifests in atypical smoldering behavior such as the observed quasi-superadiabatic effects. The value of 10.5 cm is likely specific to the liquid, sand, and column geometry used here. However, it is expected that analogous critical heights will exist and can be determined for other experimental systems.

Fig. 10 further reveals that the highest airflow rate experiment exhibits a preheating region height far in excess of 10.5 cm (21 cm at a DT=0.6) yet no atypical smoldering behavior occurred (Fig. 9b). Therefore, it is hypothesized that exceeding a critical preheating zone height is a necessary, but not sufficient, condition; atypical smoldering behavior – induced by downward organic liquid migration – also requires a reduced upward force applied by the injected air. Since temperature is the only metric available experimentally, this hypothesis is evaluated further using the analytical and numerical modeling.

3.2   Analytical Modeling of Organic Liquid Hydraulic Gradient

Using the parameter values identified in Table 2, Eq. 2 was used to estimate the magnitude and direction of the organic liquid gradient as a function of injected air flux (Table 4).

Table 5 reveals that where evidence of downward organic liquid migration was experimentally observed (forced air flux of 1.25 and 2.50 cm/s in the 90 cm columns), the analytical model

predicted a positive (i.e., downwards) organic liquid hydraulic gradient. It also indicates that at the highest air flux, the gradient is a negative (i.e., upwards), supporting the hypothesis that upward air pressure prevented downward organic liquid migration in this experiment.

3.3 Numerical Modeling of Organic Liquid Migration

The numerical model was first employed to examine the organic liquid gradient condition considered in the analytical modeling. In these simulations, it was assumed the smoldering front had advanced 10 cm from the base of the column; thus the parameters in Fig. 4 were set to A = 70 cm, B = 10 cm and C = 10 cm. Pressure plots for the organic liquid and air are very similar, demonstrating that capillary pressures are relatively small (i.e., 3 – 16%) (Appendix C, Fig. C.2); this provides support for the assumption of negligible capillary pressure in the analytical modeling.

Fig. 11 plots the organic liquid hydraulic gradient calculated from the numerically simulated heads over the 80 cm length of the contaminated zone for air fluxes from 0.1 to 8.3 cm/s. Positive (downward) organic liquid gradients were predicted for air flow rates below approximately 3.0 cm/s, which matches the experiments in which atypical smoldering was observed. Moreover, the figure demonstrates that the predictions from the numerical model and analytical model are similar in sign and magnitude in all cases. This is confirmed in Table 4, where the predicted gradient values are directly compared for the experimental conditions. The small discrepancies between the two models are likely the result of additional phenomena included in the numerical model that influence gradient including gravity and capillary pressure.

To test the hypothesis that it is the height of the preheating zone that controls migration as opposed to the overall contaminated zone height, numerical simulations were conducted with varying column heights but with no preheating zone (B=0). These results indicate that increased contaminated zone height causes a proportional increase in the air pressure at the base of the column for a given injected air flux (Appendix C, Fig. C.3) and therefore there is no effect on organic liquid hydraulic gradient (Appendix C, Fig. C.4). This suggests that total height is not in itself the key factor in determining when organic liquid migration will be significant.

In contrast, a series of numerical simulations were conducted to consider the impact of reduced viscosity in the preheating zone. These used a 90 cm column, with a 1.25 cm/s air flux, 0 cm advance of the smoldering front, and 10 cm high preheating zone (A=80, B=10, C=0). The key metric evaluated was the organic liquid volume that migrated in 20 minutes downwards into (+) or upwards away from (-) the smoldering front. In all cases the organic liquid viscosity in the ambient zone was 0.5 Pa·s (matching the experiments) while viscosity in the preheating zone was varied between 0.1, 0.01, and 0.001 Pa·s and air flux was varied from 0.1 to 8.3 cm/s. As shown in Fig. 12, high organic liquid viscosities (0.1 Pa·s) in the preheating zone resulted in relatively minimal organic liquid migration over a time scale relevant to smoldering. This corresponds with the experimental result of the 20 hour ambient temperature mobility test (Appendix A, Fig. A.1). Even at low air flow rates (<3.0 cm/s), minimal downward organic liquid migration into the smoldering front is predicted despite there being a substantial downward liquid gradient (Fig. 11). This behavior may be expected for liquids with low temperature sensitivity such as coal tar (Fig. 2). However, the organic liquid used in this study is expected to exhibit a viscosity in the preheating zone at least an order of magnitude less (~0.01 Pa.s). Fig. 12 reveals that as preheated liquid viscosity decreases to 0.01 Pa.s the predicted volume of organic liquid

migrating into the front increases by a factor of 1.7, and as it decreases to 0.001 Pa.s the migrated liquid volume increases by a factor of 13.7. These simulations lend support to the hypothesis that the presence of low-viscosity organic liquid in the preheating zone is essential for significant migration to occur in these smoldering experiments.

4 Summary and Conclusions

Laboratory self-sustaining smoldering columns demonstrated – for the first time – atypical temperature profiles that are consistent with a hypothesis of downward organic liquid mobilization. The atypical behavior included: rapid cooling and reignition events, a stall in the trailing edge of the smoldering front, a rapid increase in thickness of the smoldering front, and quasi-superadiabatic conditions leading to elevated peak temperatures. Downward organic liquid mobilization from the preheating zone into the reaction zone could explain all of these effects since the additional liquid fuel would impact temperatures in the short term and lead to energy concentration in the reaction upon ignition.

Experimental, analytical, and numerical modeling results suggested that it is necessary for three conditions to exist simultaneously for these effects to occur: (1) the forced air flux must be sufficiently low (here less than 3 cm/s) to permit a downward organic liquid hydraulic gradient to be present, (2) the viscosity of the preheated organic liquid ahead of the front must be sufficiently low (here less than 0.01 Pa.s) to enable migration to occur at a rate relevant to smoldering; and (3) the preheating zone height must be sufficiently large (here greater than 10.5 cm) to provide a sufficient volume of low-viscosity organic liquid such that the migration will influence smoldering metrics. The length of the preheating zone generally grows in time for forward smoldering, therefore, as larger columns or reactors are used (to treat larger batches of

contaminated soil), the likelihood of achieving the third condition is increased. The critical preheating zone height is likely system dependent and probably varies with organic liquid, sand grain size distribution, and other factors that affect the heat transfer and organic liquid characteristics ahead of the smoldering front.

Organic liquid mobility is expected to be minor for organic liquids whose heated viscosity is above 0.01 Pa·s (e.g., some coal tars). For other organic liquids, downward mobilization can be prevented by judiciously adjusting the air flux rate to minimize the organic liquid gradient. The appropriate value can be calculated using the analytical model presented.

The atypical smoldering behavior observed did not negate the self-sustainability of the process nor impact the very high degree of remediation of organic-contaminated sands. This reflects the robust nature of the smoldering process. It was demonstrated for the present tests that the length of the smoldering reaction zone adjusts to accommodate the influx of organic liquid from above and the trailing edge does not advance until all the liquid is consumed, leaving clean sand throughout every time. This sand is available for reuse, to be mixed with additional organic liquid and smoldered in subsequent batches. However, the processes discussed here are still important. Due to the potential for elevated peak temperatures (quasi-superadiabatic conditions) and longer treatment times, this phenomenon needs to be considered in the design of large, ex situ smoldering remediation treatment systems, including consideration of both construction materials and operating conditions.

Acknowledgements

References

[1] S.A. Leonard, J.A. Stegemann, A. Roy, Characterization of acid tars, J. Hazard. Mater. 175 (2010) 382-392.

[2] G. Hu, J. Li, G. Zeng, Recent development in the treatment of oily sludge from petroleum industry: A review, J. Hazard. Mater. 261 (2013) 470-490.

[3] C. Li, K. Suzuki, Resources, Properties and utilization of tar, Resour. Conserv. Recy. 54 (2010) 905-915.

[4] C. Switzer, P. Pironi, J.I. Gerhard, G. Rein, J.L. Torero, Self-sustaining smoldering combustion: A novel remediation process for non-aqueous-phase liquids in porous media, Environ. Sci. Technol. 43 (2009) 5871-5877.

[5] G.P. Grant, D. Major, G.C. Scholes, J. Horst, S. Hill, M.R. Klemmer, J.N. Couch, Smoldering combustion (STAR) for the treatment of contaminated soils: Examining limitations and defining success, Remediation. 26 (2016) 27-51.

[6] C. Switzer, P. Pironi, J.I. Gerhard, G. Rein, J.L. Torero, Volumetric scale-up of smouldering remediation of contaminated materials, J. Hazard Mater. 268 (2014) 51-60.

[7] P. Pironi, C. Switzer, G. Rein, A. Fuentes, J.I. Gerhard, J.L. Torero, Small-scale forward smouldering experiments for remediation of coal tar in inert media, P. Combust. Inst. 32 (2009) 1957-1964.

[8] D.A. Nield, A. Bejan, Convection in Porous Media, Springer, 2013.

[9] T.J. Ohlemiller, Modeling of smoldering combustion propagation, Prog. Energ. Combust. 11 (1985) 277-310.

[10] T.J. Ohlemiller, Smoldering Combustion, in: M.J. Hurley (Ed.), SFPE Handbook of Fire Protection Engineering, Springer (2002).

[11] G. Rein, Smouldering combustion phenomena in science and technology, Int. Rev. Chem. Eng. 1 (2009) 3-18.

[12] D.C. Walther, R.A. Anthenien, A.C. Fernandez-Pello, Smolder ignition of polyurethane foam: effect of oxygen concentration, Fire Safety J. 34 (2000) 343-359.

[13] G.C. Scholes, J.I. Gerhard, G.P. Grant, D.W. Major, J.E. Vidumsky, C. Switzer, J.L. Torero, Smoldering remediation of coal tar contaminated soil: Pilot field tests of STAR, Environ. Sci. Technol. 49 (2015) 14334-14342.

[14] S. Thomas, Enhanced oil recovery - An overview, Oil Gas Sci. Technol. 63 (2008) 9-19.

[15] A.P. Aldushin, I.E. Rumanov, B.J. Matkowsky, Maximal energy accumulation in a superadiabatic filtration combustion wave, Combust. Flame 118 (1999) 76-90.

[16] G. Rein, Smoldering Combustion, in: SFPE Handbook of Fire Protection Engineering. Springer, New York, 2016, pp. 581-603.

[17] J.I. Gerhard, T. Pang, B.H. Kueper, Time scales of DNAPL migration in sandy aquifers examined via numerical simulation, Ground Water 45 (2007) 147-157.

[18] M.C. Potter, D.C. Wiggert, Mechanics of Fluids, Brooks Cole /Thompson Learning, 2002.

[19] S.F. Kaslusky, K.S. Udell, Co-injection of air and steam for the prevention of the downward migration of DNAPLs during steam enhanced extraction: An experimental evaluation of optimum injection ratio predictions, J Contam. Hydrol. 77 (2005) 325-347.

[20] T. Rashwan, Exploration of Fuel Mobility during Self-sustaining Treatment for Active Remediation, Undergraduate Thesis, Dept. of Civil and Env. Eng., The University of Western Ontario, London, ON (2013).

[21] S.L. MacPhee, Numerical modelling of smouldering combustion for remediation of NAPL-contaminated soils, M.E.Sc. Thesis, The University of Western Ontario, London, Canada (2010).

[22] I.E. Maloka, E.T. Hashim, A.A. Hasaballah, A correlation for temperature effect on coal tar pitches and refined tars viscosity, Petrol Sci Technol. 22 (2004) 1427-1433.

[23] L. Kong, Characterization of mineral oil, coal tar and soil properties and investigation of mechanisms that affect coal tar entrapment and removal from porous media, Ph.D. Thesis, Georgia Institute of Technology, Atlanta, USA (2004).

[24] B. Esteban, J.R. Riba, G. Baquero, A. Rius, R. Puig, Temperature dependence of density and viscosity of vegetable oils, Biomass Bioenerg. 42 (2012) 164-171.

[25] T.A. Ekmondson, Effect of temperature on waterflooding, J Can Pet. 4 (1965) 236-242.

[26] J.L. Newhall, A.C. Fernandez-Pello, P.J. Pagni, Experimental observations of the effect of pressure and buoyancy on cellulose co-current smoldering, Fire Mater. 14 (1989) 145-150.

[27] W.L. McCabe, J.C. Smith, P. Harriott, Unit Operations of Chemical Engineering, McGraw-Hill, Inc, 1993.

[28] J. Bear, Dynamics of Fluids in Porous Media, Courier Corporation, 1972.

[29] R. Przybylski, T. Mag, Canola/rapeseed oil, in: F.D. Gunstone (Ed.), Vegetable Oils in Food Technology: Composition, Properties and Uses, Blackwell Publishing, CRC Press, 2002.

[30] R. Solimene, A. Marzocchella, P. Salatino, Hydrodynamic interaction between a coarse gas-emitting particle and a gas fluidized bed of finer solids, Powder Technol. 133 (2003) 79-90.

[31] N.S. Grewal, S.C. Saxena, Comparison of commonly used correlations for minimum fluidization velocity of small solid particles, Powder Technol. 26 (1980) 229-234.

[32] Bell & Mackenzie Co. Ltd. (n.d.), #12ST silica sand, Bell & Mackenzie Co. Ltd., Hamilton, ON.

[33] J.I. Gerhard, B.H. Kueper, Capillary pressure characteristics necessary for simulating DNAPL infiltration, redistribution, and immobilization in saturated porous media, Water Resour. Res. 39 (2003a) 7-1–7-17.

[34] J.I. Gerhard, B.H. Kueper, Relative permeability characteristics necessary for simulating DNAPL infiltration, redistribution, and immobilization in saturated porous media, Water Resour. Res. 39 (2003b) 8-1–8-16.

[35] J.I. Gerhard, B.H. Kueper, Influence of constitutive model parameters on the predicted migration of DNAPL in heterogeneous porous media, Water Resour. Res. 39 (2003c) 4-1–4-13.

[36] J.I. Gerhard, B.H. Kueper, G.R. Hecox, The influence of waterflood design on the recovery of mobile DNAPLs, Ground Water 36 (1998) 283-292.

[37] G.P. Grant, J.I. Gerhard, B.H. Kueper, Multidimensional validation of a numerical model for simulating a DNAPL release in heterogeneous porous media, J. Contam. Hydrol. 92 (2007) 109-128.

[38] S.L. MacPhee, J.I. Gerhard, G. Rein, A novel method for simulating smoldering propagation and its application to STAR (Self-sustaining Treatment for Active Remediation), Environ. Modell. Softw. 31 (2012) 84-98.
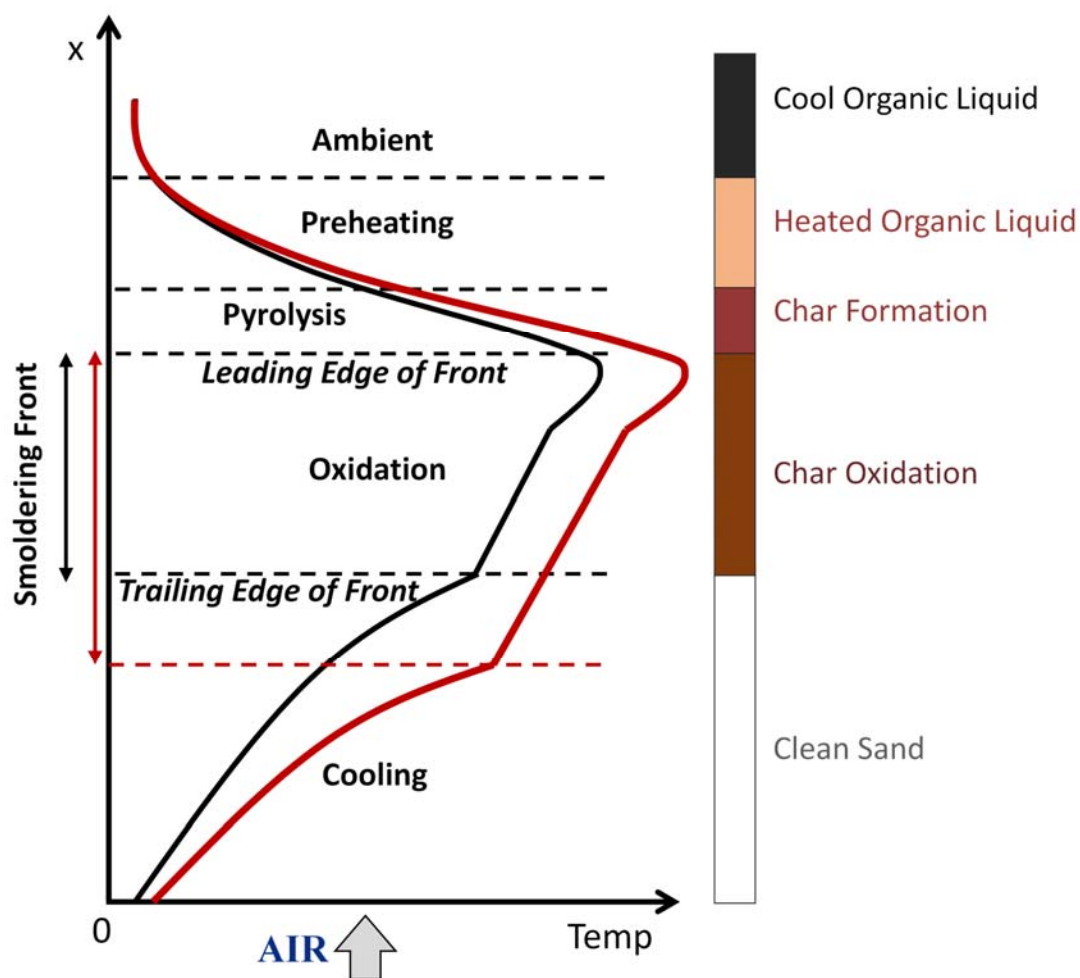
Fig. 1. Conceptual model of the distribution of temperature in a column experiencing upward, forward propagation of a smoldering reaction. The black line represents the standard model, while the red line represents how this changes in response to organic liquid migration (see Results and Discussion). The key regions dividing the front and the dividing lines that bound the front thickness are named, and the form of the organic liquid associated with each region is identified on the right hand side.
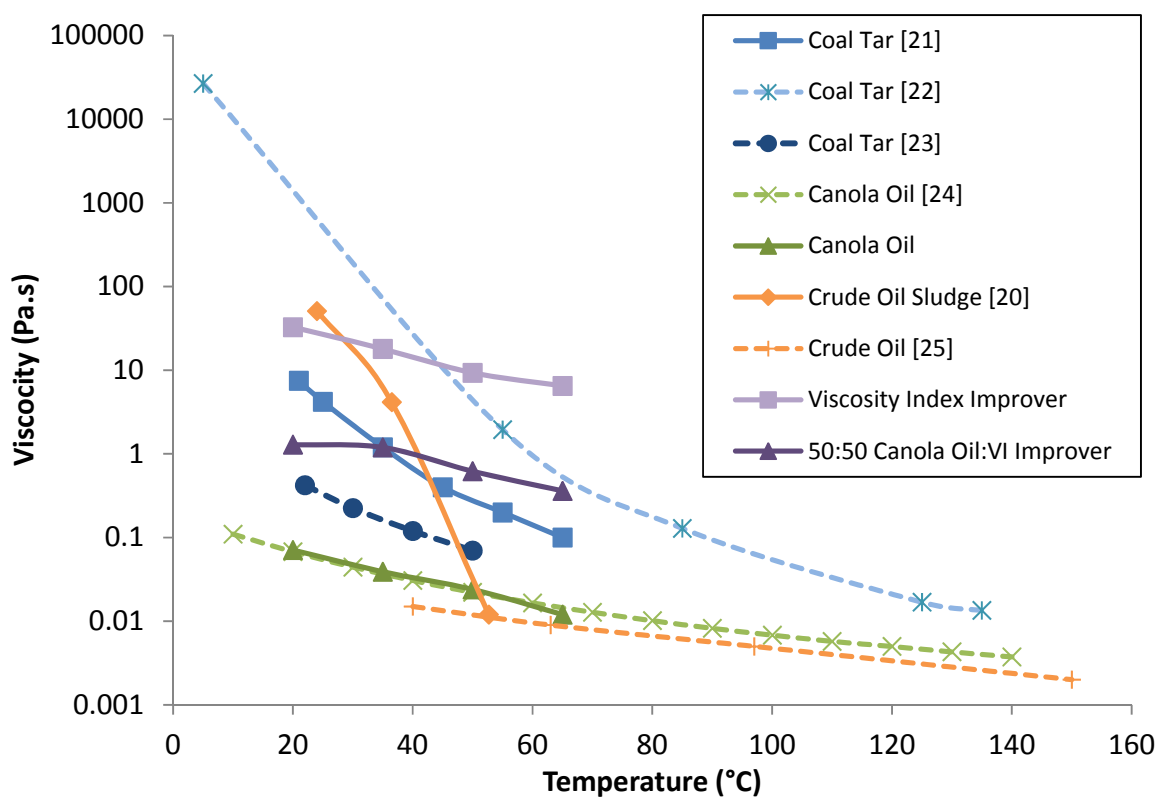
Fig. 2. Relationship between viscosity and temperature for a range of organic liquids (adapted from [20]).
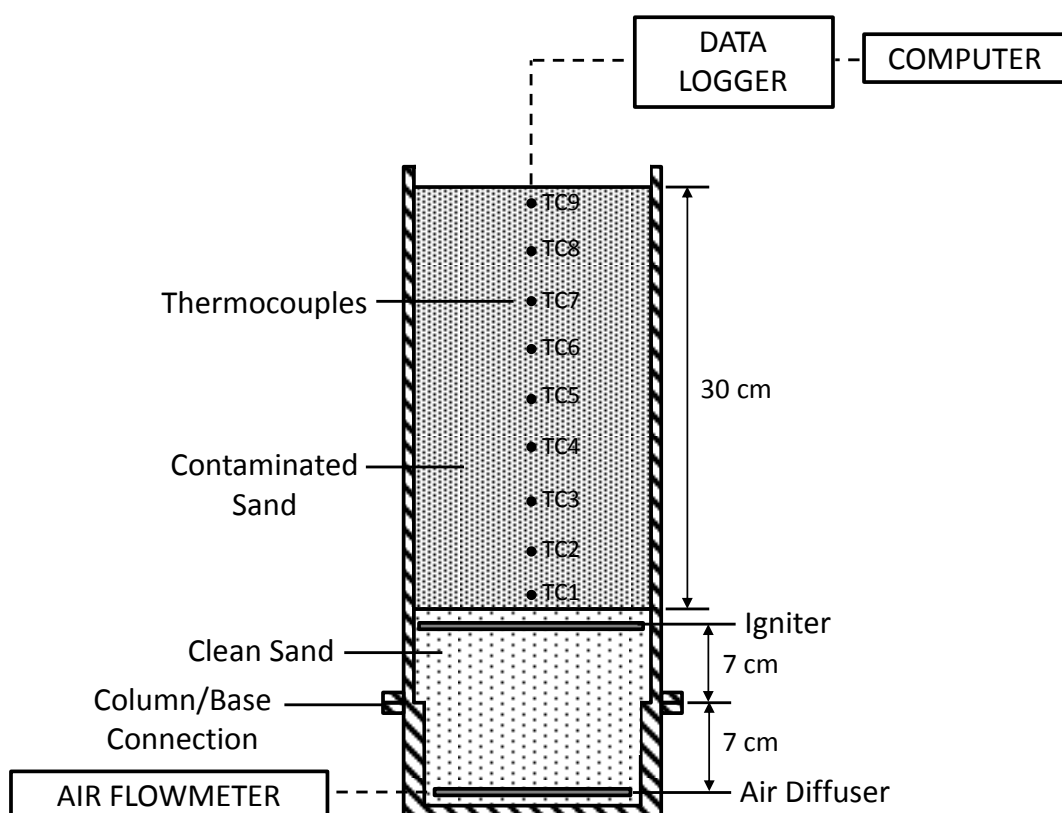
Fig. 3. Schematic diagram of the 30 cm column experimental apparatus. The 90 cm column setup consists of the same configuration, with the respective column height connected to the removable base.
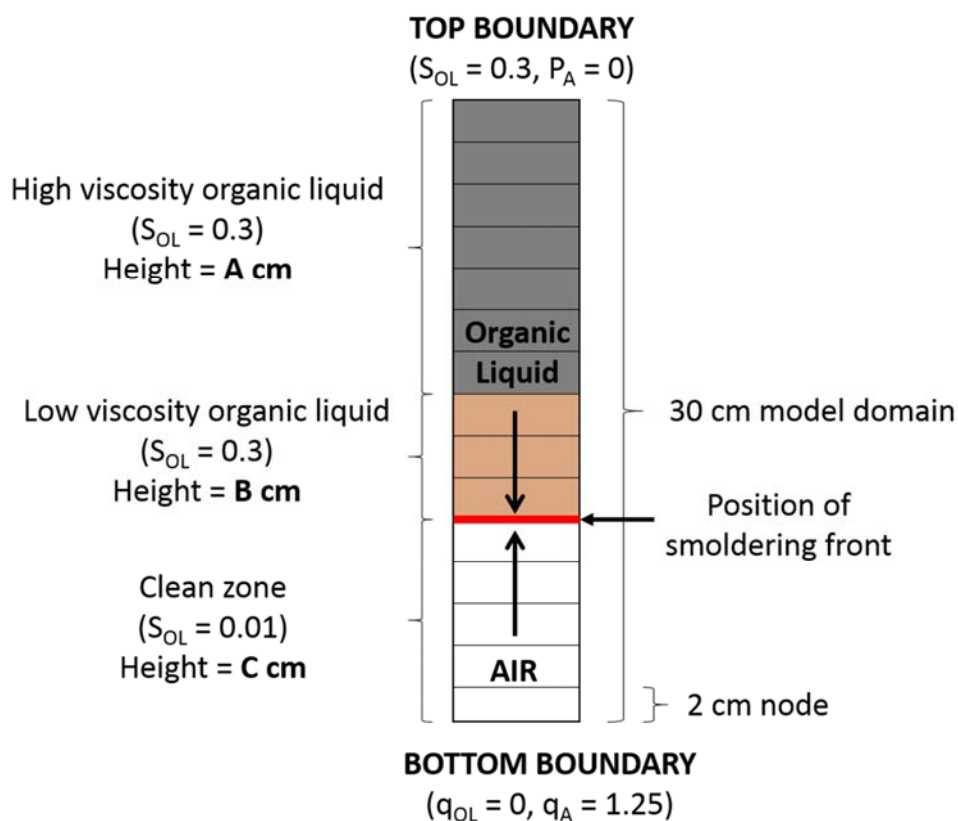
TOP BOUNDARY
($S_{OL} = 0.3$, $P_A = 0$)

High viscosity organic liquid
($S_{OL} = 0.3$)
Height = **A cm**

Low viscosity organic liquid
($S_{OL} = 0.3$)
Height = **B cm**

Clean zone
($S_{OL} = 0.01$)
Height = **C cm**

Organic
Liquid

30 cm model domain

Position of
smoldering front

AIR

2 cm node

BOTTOM BOUNDARY
($q_{OL} = 0$, $q_A = 1.25$)

Fig. 4. Sample model domain, boundary conditions and initial conditions for a 30 cm column with an initial contaminant saturation of 0.3 and a forced air flux of 1.25 cm/s. The scenario modelled is defined by: the distance C that the smoldering front has propagated from the base of the column, the height B of the elevated temperature preheating zone with reduced organic liquid viscosity, and the height A of the remaining ambient temperature (ambient viscosity) organic liquid zone.
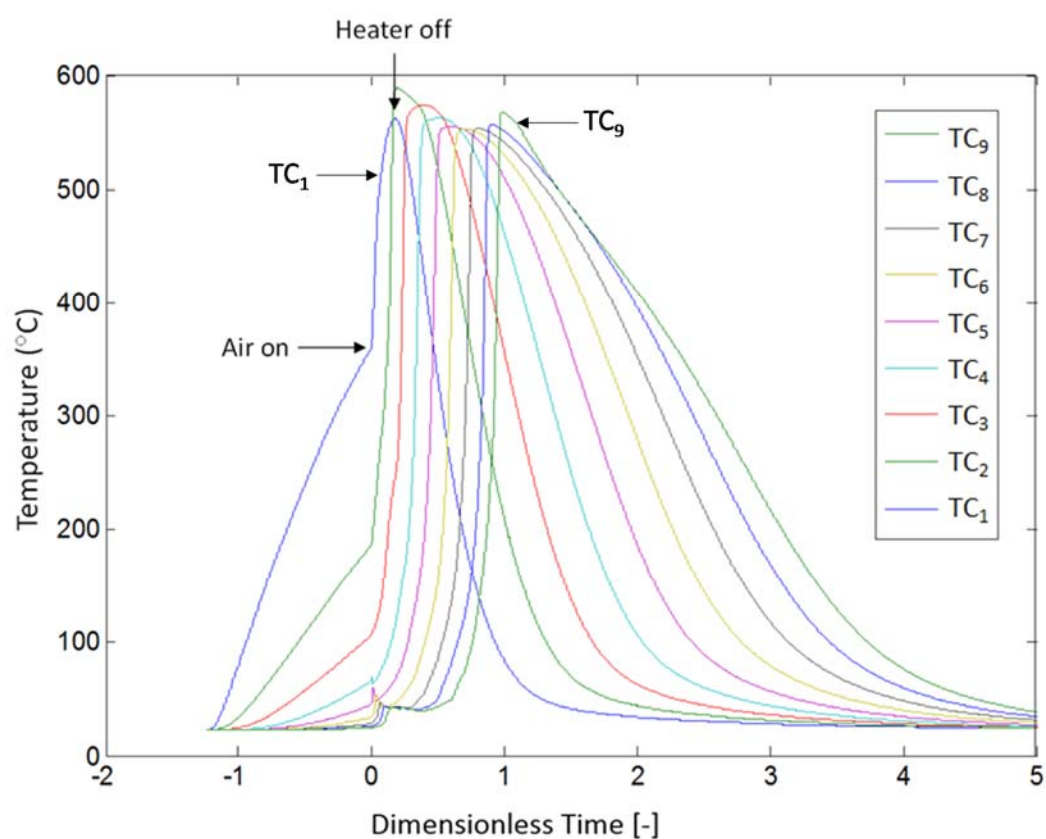
Fig. 5. Temperature history for 30 cm contaminated zone with forced air flux of 2.5 cm/s, displaying typical self-sustaining smoldering behavior in the absence of significant organic liquid migration. "Air on" represents a dimensionless time equal to 0. Thermocouples increase in temperature from ambient in order from left to right, with TC1 increasing first and TC9 increasing last.
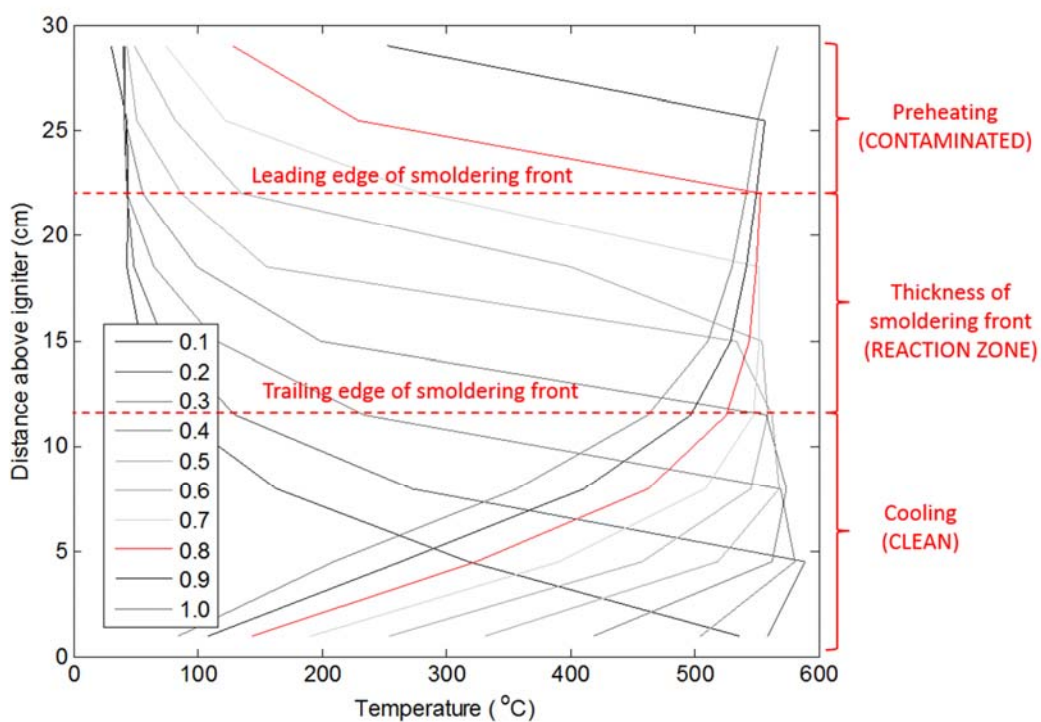
Fig. 6. Temperature profile for 30 cm contaminated zone with forced air flux of 2.5 cm/s, displaying typical self-sustaining smoldering behavior without significant organic liquid migration. The legend provides the dimensionless time for each profile. The labels refer to the smoldering regions in relation to the profile at DT = 0.8 (red plot).
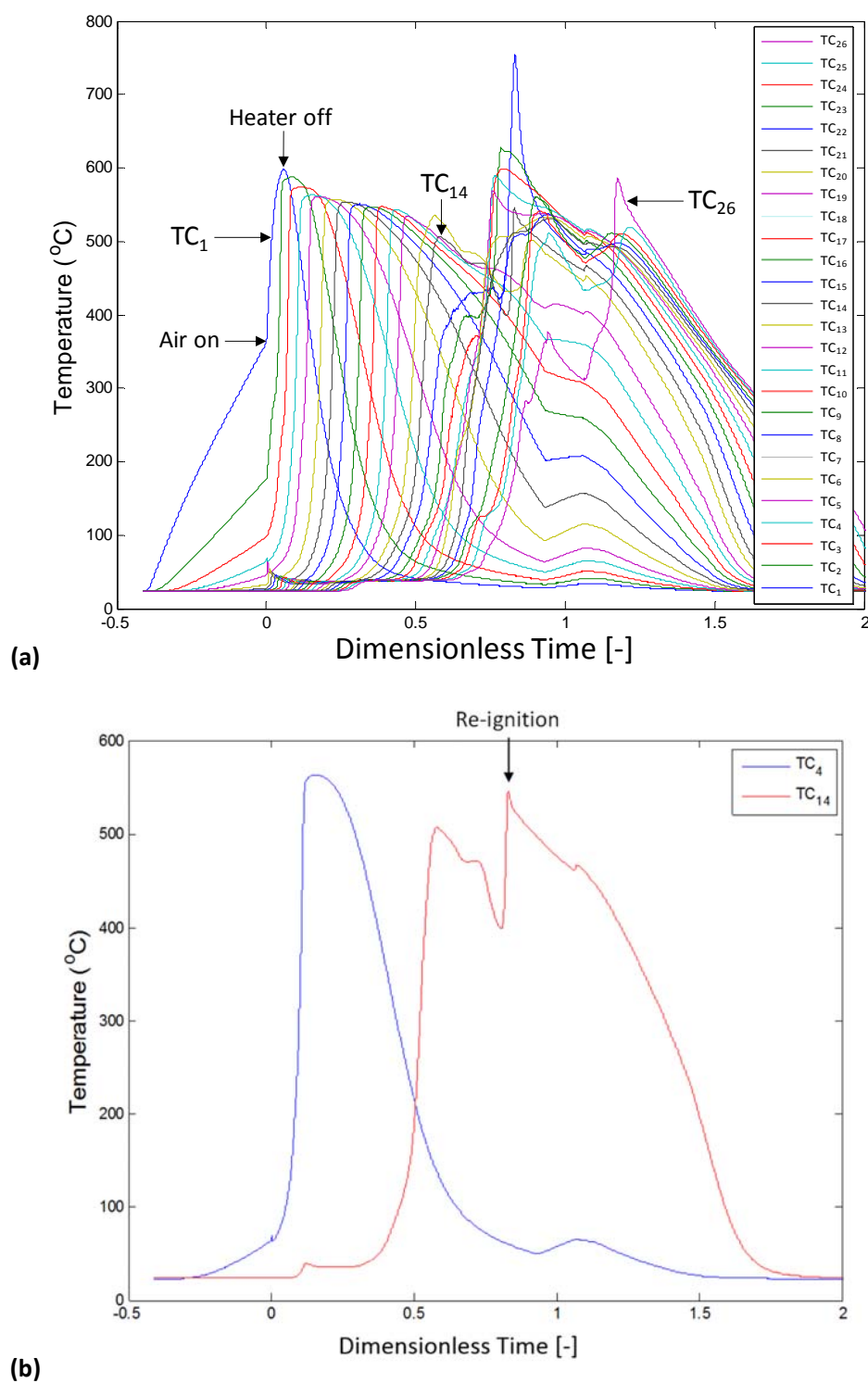
(a)

(b)

Fig. 7. (a) Temperature history for 90 cm column with forced air flux of 2.5 cm/s. Thermocouples increase in temperature from ambient in order from left to right, with TC1 increasing first and TC26 increasing last, and (b) isolated temperature history for TC4 and TC14 located 12 cm and 46.5 cm above the heater, respectively.
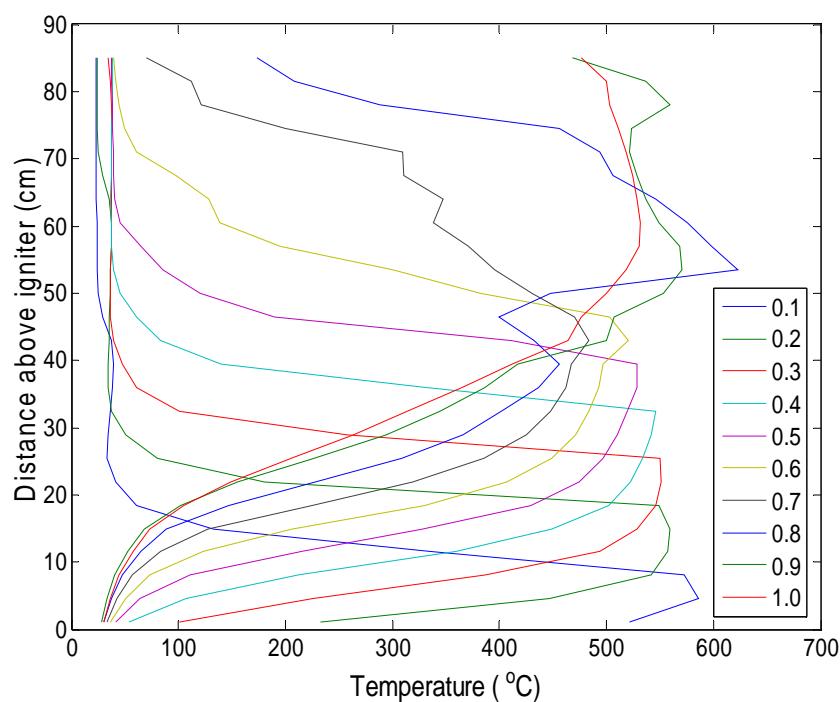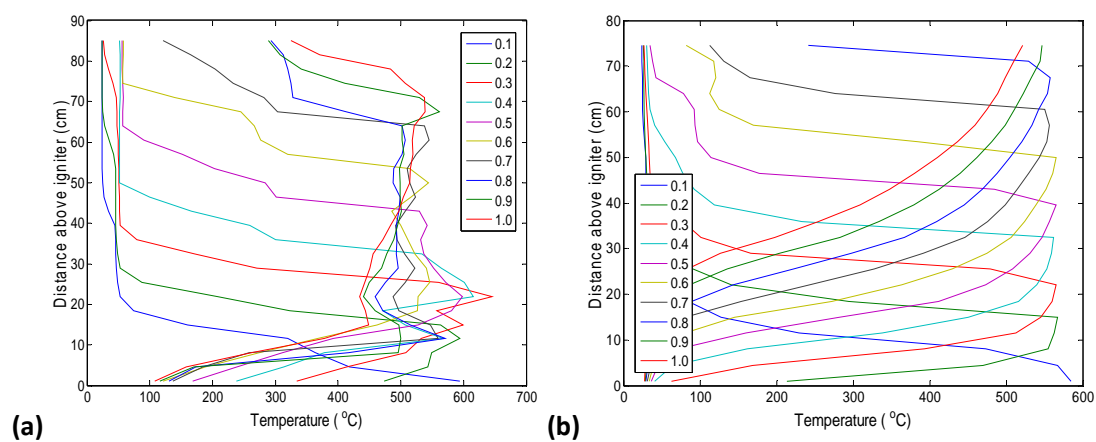
Fig. 8. Temperature profile for 90 cm column with forced air flux of 2.5 cm/s, showing evolution of the smoldering front structure. Each curve displays a snapshot in time with the legend providing the associated dimensionless time.

(a)

(b)

Fig. 9. Temperature profiles for 90 cm columns showing evolution of the smoldering front structure, with each curve displaying a snapshot in time represented as dimensionless time for forced air fluxes of (a) 1.25 cm/s, and (b) 6.25 cm/s.
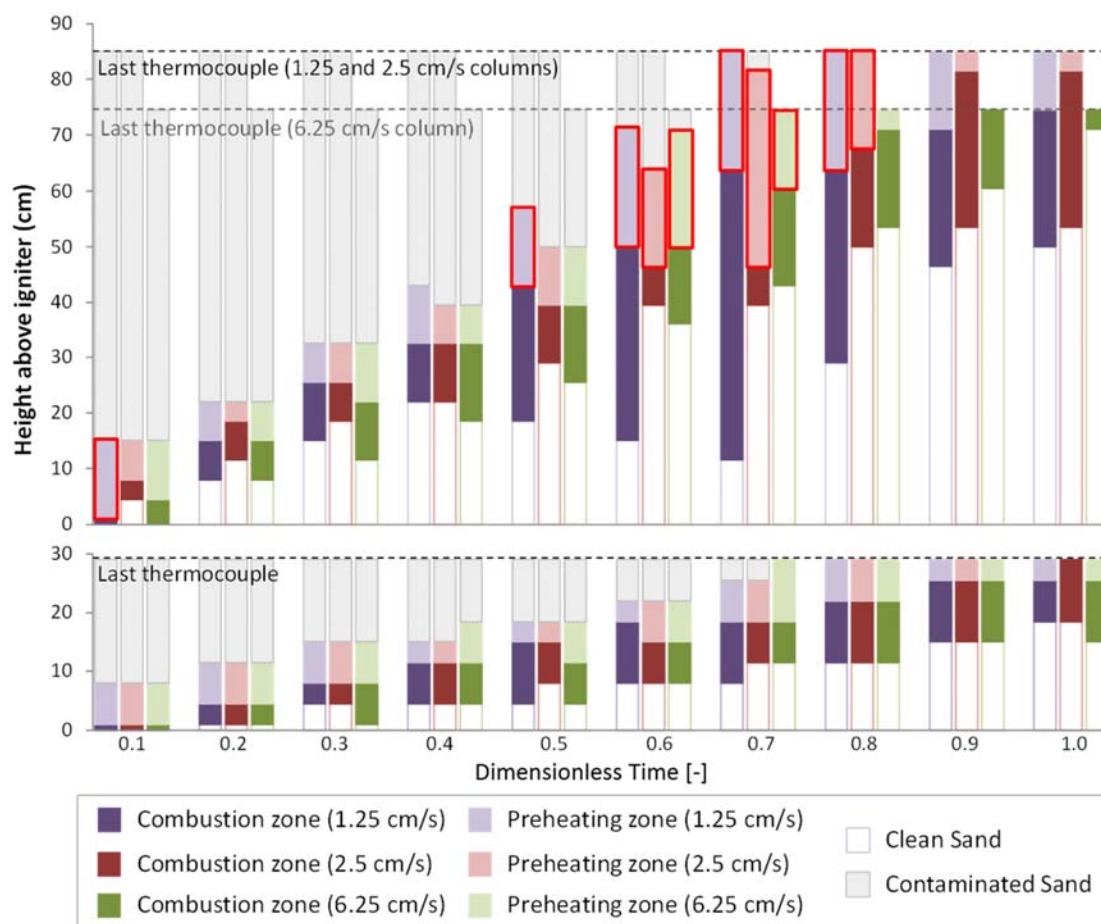
Fig. 10. Height and position of the combustion and preheating (defined as the region ahead of the combustion zone where T>100°C) zones for 30 and 90 cm columns at forced air fluxes of 1.25, 2.5 and 6.25 cm/s. The red outline identifies preheating zone heights of 10.5 cm or greater.
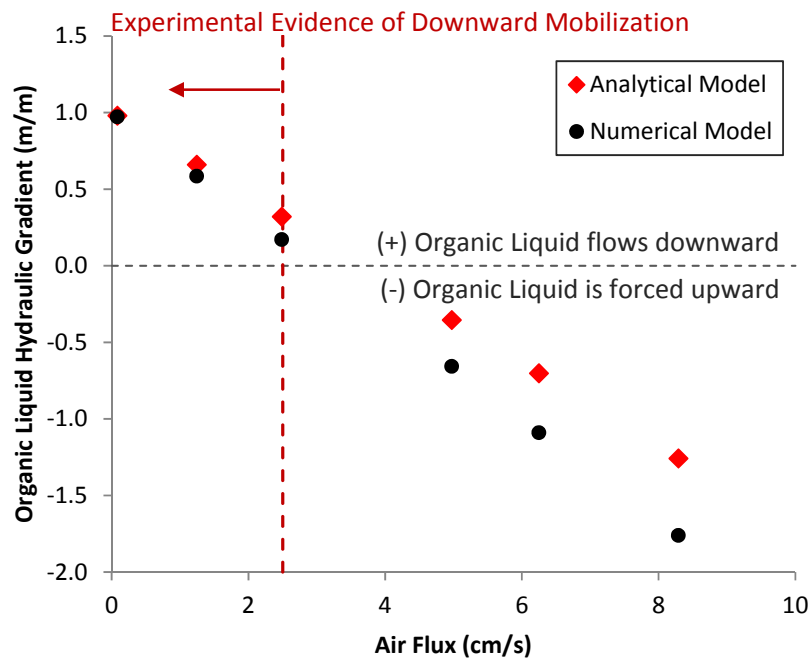
Fig. 11. Organic liquid hydraulic gradient as a function of forced air flux represented as black circles for the numerical simulations of a 90 cm contaminated zone with a 10 cm preheating zone immediately above the front (A = 80, B = 10, C = 0). Organic liquid hydraulic gradients calculated using the analytical model are shown in red.
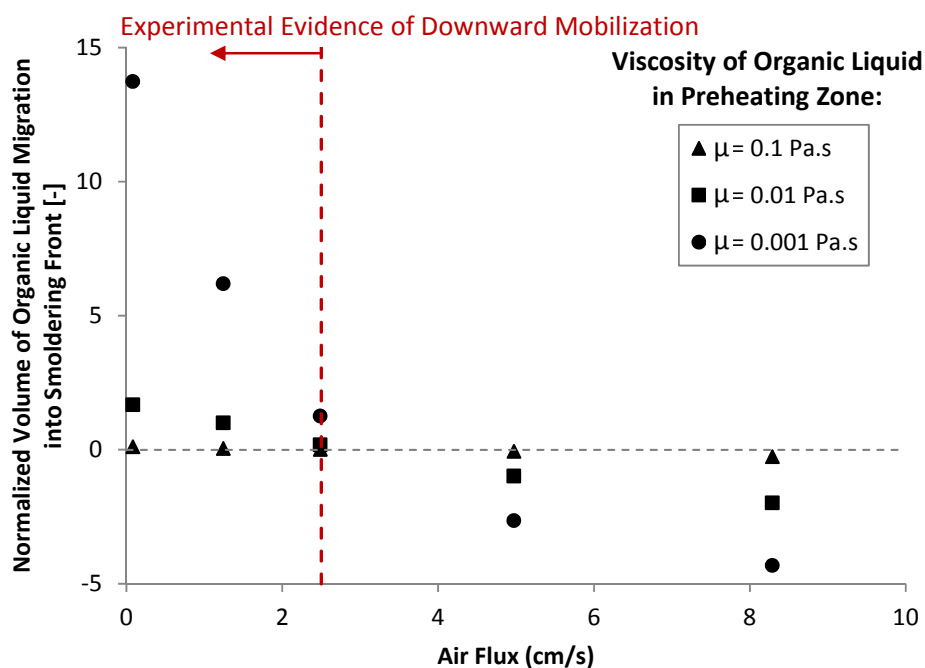
Fig. 12. Volume of organic liquid entering (+) or leaving (-) the bottom 10 cm of a 90 cm column over 20 minutes as a function of (i) forced air flux and (ii) viscosity of the organic liquid in the preheating zone. Simulation results are for a 10 cm high preheating zone located at the base of an 80 cm ambient, organic liquid-contaminated zone ($\mu = 0.5$ Pa·s), where A = 80, B = 10 and C = 0. Volumes are normalized relative to the base case (1.25 cm/s flux, $\mu = 0.01$ Pa·s).

Table 1. Summary of Smoldering Column Experiments

Test Number	Canola Oil:VI Improver (% by mass)	Organic Liquid Concentration (g/kg)	Air Flux (cm/s)	Height of Contaminated Zone (cm)
1			1.25	
2	50:50	60	2.50	30
3			6.25	
4			1.25	
5	50:50	60	2.50	90
6			6.25	

Table 2. Fluid and Porous Medium Analytical Model Parameters

Fluid and soil properties	Value
Organic liquid density (ρ_{OL})	920 (kg/m^3)[a]
Air viscosity (μ_A)	0.000025 (Pa·s)[b]
Sphericity (φ_s)	0.8[c]
Mean particle diameter (D_p)	0.88 (mm)[d]
Porosity (ε)	0.27[e]

[a] For canola oil at temperature of 20°C [29]
[b] At temperature of 200°C
[c] Approximate sphericity for silica sand [30, 31]
[d] Technical data sheet [32]
[e] Laboratory measured total porosity of 0.38 with an organic liquid saturation of 30%

Table 3. Fluid and Porous Medium Numerical Simulation Parameters

Fluid and soil properties	Value
Organic liquid density (ρ_{OL})	920 (kg/m^3)[a]
Organic liquid viscosity – high temperature (μ_{OL})	0.001 – 0.1 (Pa·s)[b]
Organic liquid viscosity – ambient temperature (μ_{OL})	0.5 (Pa·s)[b]
Air density (ρ_A)	0.75 (kg/m^3)[c]
Air viscosity (μ_A)	0.000025 (Pa·s)[c]
Interfacial tension (σ)	0.04 (N/m)
Porosity (ϕ)	0.38[d]
Residual organic liquid saturation (S_{rOL})	0.10
Emergence organic liquid saturation (S_{OL_emerg})	0.90
Pore size distribution index (λ)	2.50
Mean grain size (d)	0.88 (mm)[e]
Uniformity index (C_u)	1.6[e]
Mean permeability (k)	5.0 x10^{-10} (m^2)[f]

[a] For canola oil at temperature of 20°C [23]
[b] Brookfield DV III Rheometer

[c] At temperature of 200°C (equal to air temperature measured in the laboratory when the reaction approached the top of the column)

[d] Porosity cell (ASTM D7263)

[e] Technical data sheet [26]

[f] Pneumatic permeameter (ASTM D6539)

Table 4. Summary of Smoldering Front Velocities and Peak Temperatures

Test Number	Velocity of Leading Edge of Front (cm/s)	Velocity of Trailing Edge of Front (cm/s)	Peak Temperature (°C)
1	0.34 ± 0.06	0.24 ± 0.06	560 ± 15
2	0.41 ± 0.04	0.30 ± 0.06	564 ± 12
3	0.50 ± 0.03	0.35 ± 0.05	573 ± 14
4[1]	0.38 ± 0.07	Stalls at 10 cm	630 ± 22
5[2]	0.41 ± 0.07	Stalls at 45 cm	572 ± 60
6	0.53 ± 0.04	0.45 ± 0.08	563 ± 5

[1]Reported for bottom third (0 to 30 cm) of column, where effects of liquid migration are observed
[2]Reported for upper half (45 to 90 cm) of column, where effects of liquid migration are observed

Table 5. Predicted Organic Liquid Hydraulic Gradients in 90 cm Column Experiments

V (cm/s)	Δh/ΔL Analytical Model (m/m)	Δh/ΔL Numerical Model (m/m)	Experimental Evidence of Downward Organic Liquid Migration?
1.25	0.66	0.59	Yes
2.50	0.32	0.17	Yes
6.25	-0.70	-1.09	No